tive CO-sensitive signal transducers regulating cell functions, including cell proliferation,[10] immune responses,[11] microvascular tone, xenobiotic detoxification, and biliary excretion in the liver.[5,6,12] However, ferrous heme of these enzymes is not only sensitive to CO but to NO. In this context, whether mechanisms by which CO regulates cell and organ functions is not shared by those for NO has not fully been studied yet.

This study aimed to mine novel CO-responsive regulators for stress-inducible adaptation of metabolism. To this end, we have used metabolome analyses based on capillary electrophoresis equipped with mass spectrometry (CE-MS) for systematic mining CO-responsive gaseous signal transducers. The current results suggest that cystathionine β-synthase (CBS), the enzyme rate-limiting transsulfuration pathway is such a novel CO-sensitive regulator of metabolism that plays an important role for quality control of bile excretion under disease conditions.

Materials and Methods

Preparation of Mice. The experimental protocols herein described were approved by our institutional guidelines provided by the Animal Care Committee of Keio University School of Medicine. Mice heterozygous for disruption in the CBS gene were purchased from Jackson Labs (Bar Harbor, MI) and bred at our institution. Male heterozygous CBS-deficient mice ($CBS^{+/-}$) and their littermates ($CBS^{+/+}$), and wild-type B6J mice, which were purchased from Clea Japan, Inc (Kawasaki City, Japan), were used at 8 to 12 weeks of age. Mice were allowed free access to laboratory chow and tap water, and were fasted for 18 hours before experiments. Mice were anesthetized with an intraperitoneal injection of ketamine at 120 mg/kg, and xylidine at 6 mg/kg. Their common bile ducts were ligated in proximity to the duodenum, and the gallbladder was nicked and cannulated with a polyethylene P-10 tube to collect bile for 20 minutes after a 10-minute stabilization period.[6,13] Biliary constituents such as total bile salts, bilirubin-IXα, pH values, and bicarbonate (HCO_3^-) were measured according to previous methods described elsewhere.[13] When necessary, biliary samples were collected into tubes containing 10% trichloroacetate to measure glutathione through high-performance liquid chromatography.[14] Determination of bilirubin-IXα in bile serves as an indicator of HO-mediated heme degradation in the liver that occurs in parallel with endogenous CO generation. Hepatic CO contents were also measured by gas chromatography as described previously,[15] except that the flame ionization detector equipped with a methanizer was used in this study instead of a reduction gas detector. Combination of these methods to determine CO allowed us to distinguish endogenous CO generation from the same gas exogenously administered as an intervention as described in the following session.

Administration of Reagents Studied. Protoheme IX (hemin) was administered at 40 μmol/kg intraperitoneally at 12 hours before surgical preparation for bile collection. This protocol was denoted as liver exposed to 12-hour hemin treatment (H12) treatment in the text. After collecting bile, livers were excised immediately to be snap-frozen in cold methanol, and the lysates served as samples for contrast-enhanced time of flight/mass spectrometry analyses as described later. In separate sets of experiments, liver samples were minced with 10% trichloroacetic acid at 4°C to measure cysteine and glutathione (GSH) through high-performance liquid chromatography to confirm the data collected from contrast-enhanced time of flight/mass spectrometry, when necessary.

A series of protocols were employed to examine roles of HO-derived CO in regulation of H_2S-modulated choleresis in the H12-treated mice. First, zinc protoporphyrin, a potent HO inhibitor, was administered intravenously at 12.5 μmol/hour/kg at 30 minutes before the bile collection; this dose was sufficient to block endogenous CO in the liver. When necessary, tricarbonyldichlororuthenium (II) dimer, the CO-releasing metal carbonyl [tricarbonyldichlororuthenium (II): CORM, Sigma-Aldorich][16] was administered intraportally at 30 minutes before the start of bile collection. When necessary, CO-free ruthenium (III) chloride ($RuCl_3$) was used as a negative control reagent. To examine whether the elevation of H_2S in the liver could alter biliary HCO_3^- excretion, sodium hydrosulfide (NaHS) was administered at 20 μmol/hour/kg through the portal vein at 30 minutes before the bile collection; as seen later in Results, this protocol restored the H12-induced decrease in the hepatic H_2S contents without altering a reduction of systemic blood pressure that was induced by a systemic bolus of the NaHS injection. S-nitrosyl glutathione (GSNO) was used as an NO donor. The reagent was injected intraportally with a dose of 7 μmol/kg at 30 minutes before the collection of bile; this protocol did not induce a reduction of systemic blood pressure, whereas greater doses caused hypotension and subsequent decrease in the bile output. In these experiments, administration of the reagent was performed through a 30-gauge miniature needle that was inserted into the portal vein to be fixed at the site of puncture. Finally, to examine therapeutic effects of CO, we examined effects of H12 treatment or administration of CORM in the mice exposed to drug-induced cholestasis. To this end, cholestasis was induced by a subcutane-

ous injection of 17α-ethinylestradiol (ES) at 5 mg/kg daily for 5 consecutive days before the experiments.[17]

Metabolome Analysis. We performed metabolome analyses of tissue lysates collected from snap-frozen livers of mice using contrast-enhanced time of flight/mass spectrometry according to our previous methods.[18,19] Measurements of hepatic H_2S contents were based on gas chromatography described in our previous method.[14] Biliary flux of bilirubin-IXα (BR-IXα) in bile samples were determined by enzyme-linked immunosorbent assay using the anti–BR-IXα monoclonal antibody as described previously.[6,20] Because BR-IXα is an end product of the HO-mediated degradation of protoheme IX, its measurements in bile serves as an index of endogenous CO generation in the liver.[20] The conversion of ^{15}N-methionine to its downstream metabolites was determined by CE-MS to examine different rates of the metabolic flux through CBS in the liver. In these experiments, ^{15}N-methionine was intraperitoneally injected at 150 μmol/100 g body weight, and ^{15}N-homocysteine and ^{15}N-cystathionine were measured by CE-MS using the lysates of liver tissues at 30, 60, and 120 minutes after the methionine challenge. Data were expressed as percentages of the mass-labeled metabolites versus total amounts of metabolites in remethylation cycle [ΣRM: methionine + S-adenosyl methionine (SAM) + S-adenosyl homocysteine (SAH) + homocysteine]. In a separate set of experiments, effects of application of CO on contents of methionine and cystathionine in HepG2 cells were determined in culture. In these experiments, the cells were maintained in Roswell Park Memorial Institute 1640 medium (Invitrogen, Carlsbad, CA) containing 10% fetal bovine serum; the mixture was supplemented with 1× penicillin/streptomycin and maintained at 37°C in an atmosphere of 5% CO_2/95% air. The cells were treated with either 50 μmol/L CORM or $RuCl_3$ as a negative control for 16 hours. To measure the metabolites, a frozen pellet of the 1×10^6 cells was homogenized in 10% trichloroacetic acid with 10 mM diethylene triamine pentaacetic acid following brief centrifugation, and the supernatant was used as a sample.

Western Blot Analysis. Western blot analysis was carried out to examine an induction of heme oxygenase (HO)-1 using the polyclonal antibody SPA896 (Stressgen, Ann Arbor, MI). In these experiments, the blotting against α-tubulin was carried out using the polyclonal antibody (Cell Signaling, Danvers, MA) as an internal control.

Recombinant Full-Length Rat CBS. The complementary DNA of the full-length rat CBS was a gift from Professor Masao Ikeda-Saito in Tohoku University. Stopped-flow equipment was purchased from Unisoku, Inc. (Tokyo) and used to examine binding of CO or NO to the CBS protein according to previous methods.[21] Electron paramagnetic resonance spectrometry to determine 5-coordinated structure of the nitrosylheme complex of CBS was carried out according to previous methods.[21,22]

Statistical Analyses. The statistical significance of data among different experimental groups was determined by one-way analysis of variance and Fischer's multiple comparison test. $P < 0.05$ was considered significant.

Results

CO Overproduction Inhibits Transsulfuration and H_2S and Stimulates HCO_3^- Choleresis. Metabolome analyses based on CE-MS allowed us to pinpoint metabolic pathways responding to disease conditions. In mouse liver, we detected more than 1800 metabolites, and compared differences between the control and acetaminophen-treated livers.[18] This method was used to determine differences in metabolic responses between mouse livers and those overloaded with heme, the stressor inducing oxidative stress and subsequent CO overproduction through increasing the substrate and inducing HO-1 (Fig. 1A). The hepatic CO flux peaked at 6 hours, becoming threefold to fourfold greater during the 6 to 12 hours after challenging with hemin, as judged by BR-IXα, an end product of HO-mediated heme degradation (Fig. 1B).[13] Under these conditions, bile output was modestly but significantly increased at 12 to 18 hours after the treatment (Fig. 1C) in parallel with significant elevation of HCO_3^- to make bile more alkaline (Fig. 1D-F), enhancing solubility of organic anions during the detoxification processes. These results suggest that the heme-elicited choleretic response is not correlated with vasodilatory mechanisms by the gas. Based on these results, we used CE-MS analyses to examine metabolomics in the liver exposed to 12-hour hemin treatment (H12), in which phenotypes of bile remodeling became evident.

Among known metabolites (Table 1), most prominent differences between the control and H12 groups occurred in global decreases in amino acids concurrent with increases in Krebs cycle substrates such as acetyl CoA: the fact that these changes coincided with sustained glutamate, significant increases in glutamine, and high-energy adenosine phosphates appeared to suggest utilization of the amino acid pool for energy substrates. By contrast, several essential amino acids such as methionine, tryptophan and histidine, and serine were maintained. Another important alteration was a global decrease in transsulfuration metabolites such as cystathionine, cysteine, and

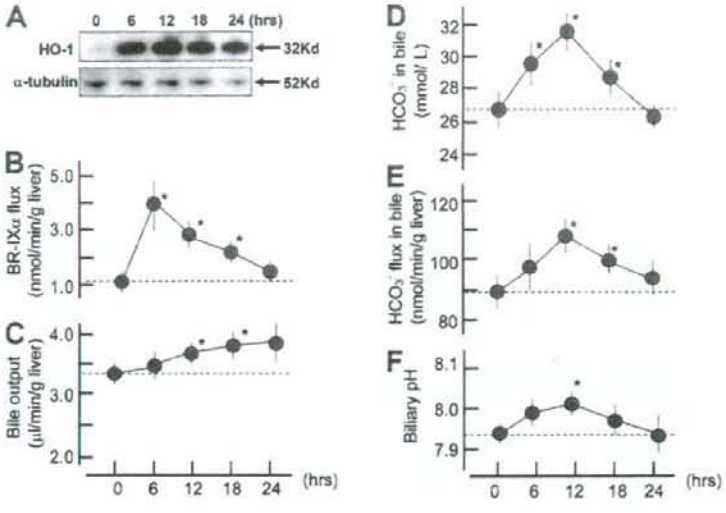

Fig. 1. Temporal alterations in hepatic generation of CO and biliary function after overloading heme. (A) Western blots indicating the induction of heme oxygenase (HO)-1. Alpha-tubulin is an internal control. (B) Biliary excretion of bilirubin-IXα (BR-IXα), a terminal metabolite of HO-dependent heme degradation, as an index of endogenous CO generation through heme oxygenase in the liver. (C) Bile output. (D) Biliary concentration of HCO_3^-. (E) Biliary flux of HCO_3^-. (F) pH values of bile. $^*P < 0.05$ versus the value measured at time 0, which is before the intraperitoneal hemin administration at 40 μmol/kg.

hypotaurine. These results led us to determine tissue contents of H_2S, the terminal product derived from CBS or cystathionine γ-lyase that constitute transsulfuration pathway; this gaseous compound turned out to be suppressed in the H12 group. Based on these measurements, we hypothesized that the H12 treatment limits the activity of CBS so far as judged from maintenance of methionine pool (ΣRM) and serine, a substrate of the enzyme, with suppression of the transsulfuration metabolites residing in the downstream (Fig. 2A). This hypothesis was confirmed by in vivo pulse-chase analysis showing accumulation of ^{15}N-homocysteine and suppression of ^{15}N-cystathionine after the ^{15}N-methionine challenge in the H12 group (Fig. 2B).

Such an inhibitory action of the H12 treatment on the transsulfuration pathway was reproducible when HepG2 cells was treated with CO in culture; contents of cystathionine were significantly suppressed by the application of 50 μmol/L CORM (9.3 ± 1.3 versus 15.9 ± 1.4 nmol/g protein for the vehicle treatment with $RuCl_3$. Mean ± standard error (SE) of three separate experiments, $P < 0.03$), whereas methionine exhibited no difference (66.3 ± 3.7 versus 80.3 ± 12.2 nmol/g protein for CORM and $RuCl_3$, respectively. Mean ± SE of three separate experiments), suggesting inhibitory action of the gas on CBS.

CO But Not NO Inhibits CBS. H12-induced metabolomic changes indicating dissociation between remethylation cycle and transsulfuration pathway led us to hypothesize that CBS, a heme-containing enzyme that rate-limits the transsulfuration pathway, is a sensor of the H12-elicited CO overproduction. Rat full-length recombinant CBS were purified (Fig. 3A) to examine whether CO or NO could inhibit the enzyme activities. CO, but not NO, specifically inhibited the enzyme (Fig. 3B). Previous crystallographic studies using a truncated form of CBS showed that the axial ligands for the prosthetic heme were cysteine and histidine, indicating a large peak of absorbance at 448 nm.[23] On CO application, the heme formed a 6-coordinated CO-Fe(II)–histidine complex, as judged by a decrease in the absorbance at 448 nm and a reciprocal elevation at 422 nm (Fig. 3C). These results were consistent with previous works using the truncated form of human recombinant CBS.[24] Such an inhibitory effect of CO on CBS activity occurred even when sufficient amounts of SAM were present as an allosteric activator,[25] whereas the CO concentrations necessary to suppress CBS became greater in the presence of SAM (Fig. 3D). Conversely, NO was able to bind to the heme but with a distinct structure of 5-coordinated nitrosyl-heme as judged by electron paramagnetic resonance spectrometry (Fig. 3E), suggesting that the enzyme responds specifically to the binding of CO but not that of NO.

CO-Induced HCO_3^- Choleresis Is Sensitive to H_2S and Disappears in $CBS^{+/-}$ Mice. Recent studies indicated that H_2S derived from cystathionine γ-lyase, an enzyme using cysteine to generate the gas, modulates biliary HCO_3^- excretion via mechanisms involving glibenclamide-sensitive channels, a putative H_2S target.[14,26] We hypothesized that the stress-induced CO stimulates the HCO_3^- excretion to increase pH in bile through its inhibitory action on CBS-derived H_2S. To examine this hypothesis, we chose the dose of the CO-releasing molecule (CORM) that was able to increase hepatic contents

Table 1. Comparison of Metabolome Analysis by CE-MS in Liver Extracts Between Control and the Hemin-Treated (H12) Mice

	Control	H12
Carbohydrates (nmol/g liver)		
Glucose 1-P	20 ± 4	31 ± 5
Glucose 6-P	24 ± 1	22 ± 6
Ribulose 5-P	206 ± 60	115 ± 17
Fructose 6-P	25 ± 1	21 ± 6
Glycerol 3-P	1800 ± 250	1663 ± 218
Lactate	3490 ± 633	2920 ± 385
Acetyl CoA	3.4 ± 0.5	6.2 ± 1.1*
Malonyl CoA	37 ± 6	83 ± 15*
Citrate	70 ± 13	88 ± 20
Fumarate	120 ± 22	167 ± 52
Malate	343 ± 91	479 ± 90
CoA	132 ± 21	111 ± 20
Nucleotides (nmol/g liver)		
ATP	208 ± 35	480 ± 90*
GTP	33 ± 4	79 ± 14*
ADP	577 ± 104	1060 ± 154*
AMP	1866 ± 277	1863 ± 70
IMP	501 ± 82	660 ± 99
Adenosine	203 ± 18	151 ± 11
Adenine	12 ± 1	12 ± 2
Hypoxanthine	58 ± 8	43 ± 15
	Control	**H12**
Amino acids (μmol/g liver)		
Gly	3.16 ± 0.11	2.20 ± 0.05*
Ala	3.12 ± 0.48	1.47 ± 0.40*
Ser	0.38 ± 0.07	0.31 ± 0.05
Pro	0.37 ± 0.03	0.27 ± 0.04*
Val	0.41 ± 0.01	0.23 ± 0.05*
Thr	0.31 ± 0.03	0.20 ± 0.04*
Lys	0.69 ± 0.13	0.46 ± 0.05*
Cys	0.20 ± 0.04	0.07 ± 0.03*
Leu	0.36 ± 0.02	0.25 ± 0.05†
Asp	0.76 ± 0.13	0.59 ± 0.12†
Glu	2.90 ± 0.16	2.75 ± 0.28
Gln	3.39 ± 0.58	6.48 ± 0.54*
His	0.43 ± 0.05	0.48 ± 0.02
Amino acids and derivatives (nmol/g liver)		
Met	49 ± 5	39 ± 10
GABA	29 ± 2	25 ± 4
Ornithine	420 ± 95	226 ± 22*
Asn	77 ± 7	59 ± 3*
Ile	175 ± 12	94 ± 17*
Arg	8.8 ± 1.2	4.8 ± 0.6*
Citrulline	64 ± 10	35 ± 3*
Trp	34 ± 2	31 ± 3
Tyr	111 ± 15	52 ± 8*
Glu-2 aminobutyrate	6.3 ± 2.3	5.7 ± 1.2
Ophthalmate	67 ± 7	83 ± 6

Data indicate mean ± SE of six separate experiments.

Data of metabolites in remethylation cycle and transsulfuration pathway were indicated in Fig. 2A.

*$P < 0.05$ and †$P < 0.1$ versus controls.

of CO comparably to those measured in the H12 treatment: As seen (Fig. 4A), the intraportal administration of CORM at 20 μmol/kg significantly increased hepatic CO contents comparable to those induced by H12 treatment in the intact mice. This dose of CORM suppressed hepatic H_2S and stimulated biliary HCO_3^- flux. Stimulatory effects of CO administration on biliary HCO_3^- excretion in intact mice were not shared by NO, as judged by observation in the mice administered with GSNO, an NO donor (Fig. 4B): These results were consistent with observation that CBS is sensitive to CO but not to NO in vitro (Fig. 3).

As already seen, H12 treatment increased CO generation (biliary BR-IXα flux), decreased hepatic H_2S contents, and stimulated biliary HCO_3^- flux (Fig. 1). HO blockade by zinc protoporphyrin-IX cancelled these changes elicited by H12 treatment. On the other hand, an administration of NaHS, an H_2S donor, abolished the H12-induced suppression of hepatic H_2S contents, and significantly attenuated the stimulatory response of biliary HCO_3^- flux (Fig. 5A), suggesting that H12-inducible CO stimulates biliary HCO_3^- excretion through modulation of CBS-derived H_2S. As previously reported, homozygous CBS knockout mice died of severe hepatic steatosis, whereas heterozygous knockout ($CBS^{+/-}$) mice survive through compensation without apparent phenotypes.[27] In these mice, indeed, the baseline H_2S content in livers of $CBS^{+/-}$ mice was comparable to that of $CBS^{+/+}$ mice, presumably because of compensation of the gas generation through cystathionine γ-lyase. On H12 treatment, $CBS^{+/-}$ mice exhibited an increase in the hepatic CO generation comparably to $CBS^{+/+}$ mice, but neither decreased H_2S contents nor up-regulated biliary HCO_3^- flux (Fig. 5B), indicating phenotypes distinct from those in $CBS^{+/+}$ littermates.

CO Protects Against Drug-Induced Cholestasis Through Mechanisms Involving CBS. We further attempted to investigate whether the administration of CO could improve biliary dysfunction occurring in disease models. To examine this, the mice were treated with ES, a cholestatic reagent suppressing three major osmolites such as HCO_3^-, glutathione, and bile salts in bile.[17] H12 treatment or the administration of CORM significantly increased bile output concurrently with a recovery of HCO_3^- excretion into bile (Fig. 6A). The anti-cholestatic effects of H12 treatment through stimulation of HCO_3^- excretion disappeared in the $CBS^{+/-}$ mice (Fig. 6B), suggesting again a pivotal role of CBS for triggering the CO-induced choleresis.

Discussion

CO administration or HO-1 induction has been shown to protect against tissue injury and considered a potentially useful therapeutic stratagem.[8,16] Serendipitous observation in the liver indicating effects of overproduced CO on metabolism of sulfur-containing amino

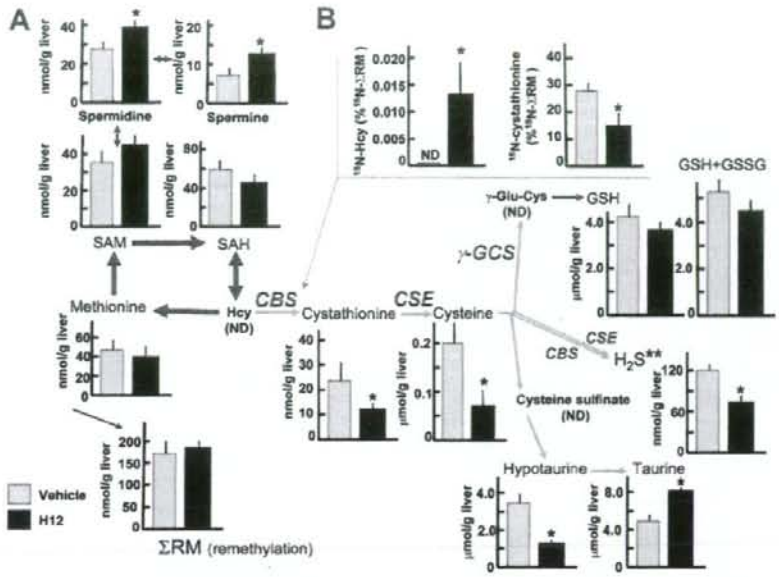

Fig. 2. Metabolomic comparison of sulfur-containing amino acids and their derivatives between the heme-overloaded and vehicle-treated livers of mice. (A) Differences in hepatic contents of the metabolites between the control and hemin-treated mice. H12: treatment with hemin at 12 hours before sampling the liver. Note decreases in transsulfuration metabolites. (B) *In vivo* pulse-chase analysis indicating conversion rates of ^{15}N-methionine into ^{15}N-homocysteine (Hcy) and ^{15}N-cystathionine in livers between the groups. The amounts of the downstream metabolites were measured at 30 minutes after the methionine administration. The data in B were normalized by total amounts of metabolites in remethylation cycle (^{15}N-methionine + ^{15}N-SAM + ^{15}N-SAH + ^{15}N-Hcy = ΣRM) at 30 minutes. ND, not detected. Data indicate mean ± SE of six to eight separate experiments for each group. *$P < 0.05$ versus the vehicle-treated group.

acids led us to reveal unique physiological actions of this gas on CBS *in vivo* that are not shared with NO. The current study suggested that stress-inducible CO targets CBS and thereby reduces H_2S significantly to stimulate biliary HCO_3^- excretion that could benefit detoxification processes. Conversely, such a property of stress-inducible CO might jeopardize anti-oxidative defense systems through an overflow of homocysteine or through a shortage of GSH. Under current experimental conditions, however, such a risk seemed little, if any, so far as judged from maintenance of GSH and adenosine triphosphate so far. This appears to result from large difference in amino acid pools between methionine (nmol/g) and thiols including cysteine and GSH (μmol/g). Furthermore, cysteine could be supplied through its uptake from extracellular space by mechanisms involving Nrf2, the transcriptional factor activated in response to oxidative stress or electrophiles such as heme.[28,29] By contrast, the amounts of sulfur-containing amino acids consumed to generate H_2S seems relatively smaller than that for synthesizing GSH or hypotaurine, as judged from quantitative information collected by metabolome analysis. Because CBS not only limits synthesis of cystathionine from homocysteine but also directly suppresses H_2S generation from cysteine, the inhibitory effects of CO on the enzyme could dictate largely on the action of H_2S in the liver, causing a stimulatory effect on bile excretion. Considering recent studies suggesting vasodilatory effects of H_2S,[26,30] suppression of CBS-derived H_2S by stress-inducible CO might trigger vasoconstriction, but such vasoactive responses did not occur so far as judged from choleretic response of the basal bile flow that is highly dictated by microvascular perfusion. This might result from the fact that stress-inducible CO itself has the ability to maintain the basal microvascular perfusion through multiple vasodilatory mechanisms involving activation of cyclic guanosine monophosphate and modulation of cytochrome P450–derived vasoconstrictors.[6,20,31]

Although the inhibitory action of stress-inducible CO on the transsulfuration pathway has first been shown in the heme-overloading detoxification model of mice in the current study, a similar event occurred in acetaminophen-induced acute liver injury model of mice in which CO was overproduced through degradation of cytochrome P450–derived heme.[5,18] Our previous study in rats suggested that another HO-derived product bilirubin but not CO

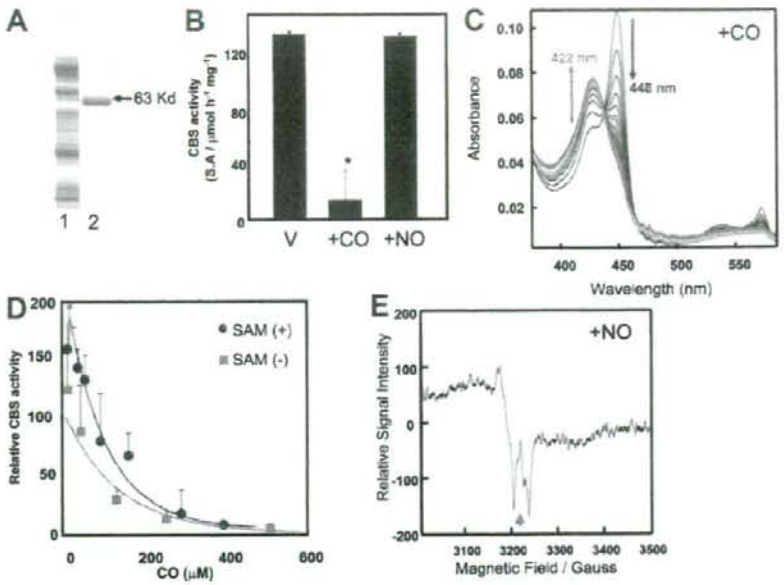

Fig. 3. Effects of CO and NO on the activity and structure of the prosthetic heme of rat recombinant full-length CBS. (A) Sodium dodecyl sulfate polyacrylamide gel electrophoresis for purification of rat recombinant CBS. Lane 1, crude extract; lane 2, purified CBS. (B) Effects of CO and NO on the Fe(II)-CBS activity under optimal substrate conditions at pH 7.4. CO but not NO (100 μM) significantly attenuated the activities of the ferrous enzyme. Data indicate mean $\pm$ SE of four experiments. The activities were measured by determining conversion of homocysteine and serine to cystathionine. $^*P < 0.05$ versus the group treated with vehicle (V). The concentration of CBS-heme was 10 μM. (C) Stopped-flow visible spectrophotometry for Fe(II)-CBS to examine temporal transitional changes after mixing with CO. Data exhibited a drop at 449 nm and a reciprocal elevation at 422 nm, demonstrating stabilization of the 6-coordinated CO-Fe(II)-histidine complex. $K_{obs} = 0.638$/second. (D) Effects of CO on the CBS activities in the presence or absence of S-adenosyl methionine (SAM), the allosteric activator of the enzyme. (E) Electron spin resonance spectrometry indicating 5-coordinated NO-Fe(II) complex of the CBS-heme. Arrow: g-value = 2.008.

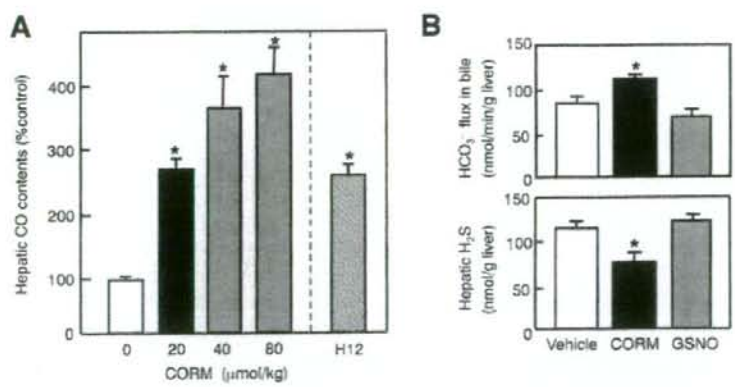

Fig. 4. Effects of the administration of CORM on hepatic CO delivery and biliary function, and their comparison with GSNO, an NO donor. (A) Effects of administration of CORM on hepatic CO contents. H12: the CO contents measured at 12 hours after an intraperitoneal injection of hemin at 40 μmol/kg. Data indicate mean $\pm$ SE of five separate experiments for each group. $^*P < 0.05$ versus the controls. Note that 20 μmol/kg CORM caused an increase comparable to that induced by H12. (B) Effects of an intraportal administration of CORM on hepatic H_2S contents and biliary HCO_3^- flux. GSNO, S-nitrosyl glutathione, an NO donor. $^*P < 0.05$ versus the values in the vehicle-treated controls. Data indicate mean $\pm$ SE of seven to eight separate experiments for each group.

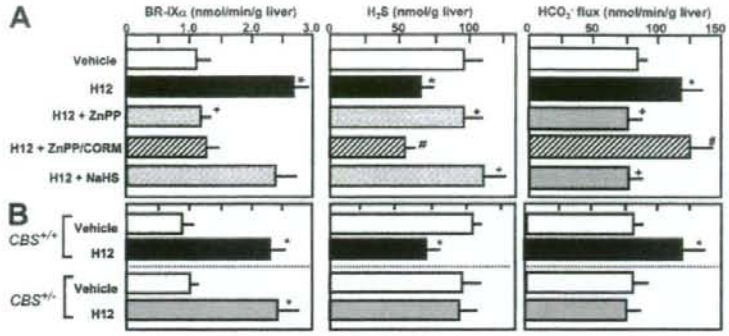

Fig. 5. Effects of HO blockade by zinc protoporphyrin and supplementation of NaHS, an H_2S donor, on biliary flux of BR-IXα, hepatic H_2S contents, and biliary HCO_3^- excretion in the 12-hour hemin-treated liver (H12). (A) Measurements in wild-type male B6 mice. Note that the hemin-induced suppression of H_2S generation and stimulation of biliary HCO_3^- excretion were sensitive to the HO inhibitor and reversed by supplementing CO (CORM). An injection of NaHS, an H_2S donor, restored hepatic H_2S contents and repressed the biliary HCO_3^- excretion in the H12-treated liver, suggesting that the biliary response is H_2S-dependent. (B) Disappearance of H12-induced reduction of H_2S and biliary HCO_3^- excretion in heterozygous CBS-knockout mice ($CBS^{+/-}$). Note that $CBS^{+/-}$ mice neither exhibit a reduction of H_2S nor up-regulate biliary HCO_3^- excretion, although overproducing CO (BR-IXα flux) comparably to the littermates ($CBS^{-/-}$). *$P < 0.05$ versus the vehicle-treated controls. +$P < 0.05$ versus the H12-treated groups. #$P < 0.05$ versus the H12+ zinc protoporphyrin-treated groups.

has the ability to improve bile acid–dependent bile output of the post–cold ischemic liver grafts through its antioxidative action.[32] However, such an effect of bilirubin appears to be distinct from the stimulatory action of CO on biliary fluid excretion indicated in the current study. CO has been shown to exert diverse actions on biliary function through multiple mechanisms: First, stress-inducible levels of CO have the ability to elongate the intervals of bile canalicular contraction, which helps increase the stroke volume for promoting bile excretion; this process appears to involve mechanisms mediated by modulation of cytochrome P450 epoxygenases and intra-

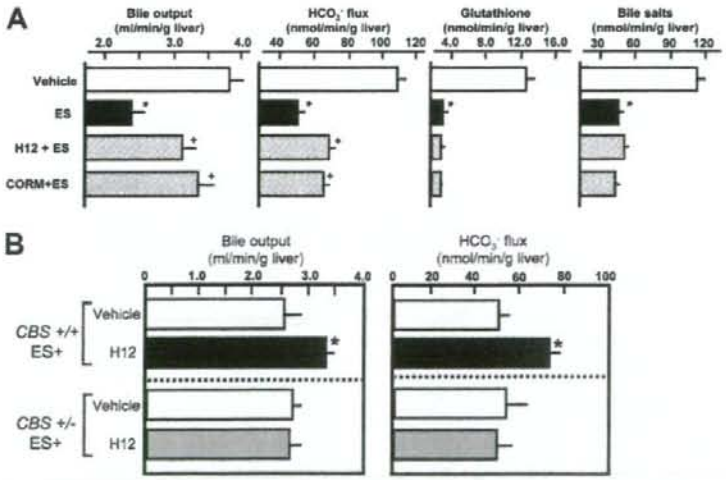

Fig. 6. Effects of H12 treatment or CORM administration on 17α-ethinylestradiol (ES)-induced cholestasis in male B6 mice. (A) Effects of H12 or CORM on ES-induced decreases in the bile output and bile constituents. ES elicited marked cholestasis, which coincided with decreases in HCO_3^-, glutathione, and bile salts in bile. Pretreatment with hemin at 12 hours before the administration of ES (H12 + ES) or the administration of CORM significantly attenuated ES-induced cholestasis through stimulation of HCO_3^- excretion into bile. (B) Effects of H12 treatment on ES-induced impairment of bile output and biliary HCO_3^- flux in $CBS^{+/+}$ and $CBS^{+/-}$ mice. *$P < 0.05$ versus the values in vehicle-treated controls. +$P < 0.05$ versus the values in ES-treated group. Data indicate mean ± SE of eight separate experiments for each group. Note disappearance of the improving effect of H12 treatment in the $CBS^{+/-}$ mice.

cellular Ca^{2+} mobilization.[12] Second, suppression of endogenous CO activates bile acid–dependent bile excretion through accelerated vesicular transport of taurocholate, while inducing no significant elevation of the bile acid–independent fraction.[33] Conversely, CO overproduction by the HO-1 induction or exogenous administration of CO stimulates bile acid–independent choleresis concurrently with increased mrp2-dependent excretion of bilirubin-IXα and glutathione, while suppressing biliary excretion of bile salts, indicating the effects of the gas for stimulating fluid excretion into bile.[34] Of interest is that glibenclamide, an inhibitor of K^+ channel that serves as a putative target for H_2S,[26] acts on Na^+-K^+-$2Cl^-$ cotransporter in bile duct epithelium to stimulate biliary HCO_3^- excretion in normal and cholestatic livers.[35] We showed that inhibition of cystathionine γ-lyase, another H_2S-generating enzyme, stimulates basal and glibenclamide-induced fluid output of bile through stimulating HCO_3^- excretion without altering the baseline vascular resistance of the liver.[14] Recent studies provided evidence that such a glibenclamide-responsive channel is present in rodent cholangiocytes[36] or in duodenum,[37] contributing to stimulation of the HCO_3^- excretion.[36] Based on these observations, it is not unreasonable to speculate that CO stimulates biliary fluid excretion through mechanisms involving H_2S-mediated modulation of glibenclamide-sensitive channels on biliary epithelium. Although further investigation is necessary to determine whether these mechanisms are sensitive to H_2S, the current results shed light on a possibility that the CO-CBS system serves as a putative mechanism for stimulating bile acid–independent fluid excretion, facilitating excretion of HCO_3^- and organic anions such as bilirubin to support heme detoxification. Both glibenclamide and CO help biliary fluid excretion in estrogen-induced hepatocellular cholestasis. Exploration of H_2S-sensitive molecular targets occurring on biliary epithelium deserves further studies for evidence that HO-1–derived CO serves as a therapeutic stratagem for protecting against cholestasis.

CO has been believed to share varied physiological effects on biological systems with NO. However, through extrapolation of studies *in vitro* indicating biochemical actions of CO to trigger structural changes in gas-responsive heme proteins (such as sGC, hemoglobin) distinct from those elicited by NO,[7,19,21,22,38] evidence that CO is a unique gaseous regulator distinct from NO has been emerging. In fact, CO itself modestly activates sGC, by which hepatic sinusoids are constitutively dilated.[2,20,39] By contrast, in vascular smooth muscle cells in which NO is sufficiently supplied from arteriolar endothelium (for example, brain microcirculation), the inducible CO inhibits NO-elicited sGC activation.[40,41] Besides these observations suggesting physiologic actions of CO occurring dependently of local NO levels, the current study provided evidence for a novel mechanism functioning irrespective of the NO effects. Furthermore, our results shed light on a metabolic link between CO and H_2S, suggesting that different gaseous mediators constitute an intriguing link for regulation of organ functions.

Acknowledgment: The authors thank Kayo Maruyama for technical support in measuring tissue H_2S contents.

References

1. Verma A, Hirsch DJ, Glatt CE, Ronnett GV, Snyder SH. Carbon monoxide: a putative neural messenger. Science 1993;259:381-384.
2. Suematsu M, Goda N, Sano T, Kashiwagi S, Egawa T, Shinoda Y, et al. Carbon monoxide: an endogenous modulator of sinusoidal tone in the perfused rat liver. J Clin Invest 1995;96:2431-2437.
3. Ozawa N, Goda N, Makino N, Yamaguchi T, Yoshimura Y, Suematsu M. Leydig cell-derived heme oxygenase-1 regulates apoptosis of premeiotic germ cells in response to stress. J Clin Invest 2002;109:457-467.
4. Song R, Zhou Z, Kim PK, Shapiro RA, Liu F, Ferran C, et al. Carbon monoxide promotes Fas/CD95-induced apoptosis in Jurkat cells. J Biol Chem 2004;279:44327-44334.
5. Mori M, Suematsu M, Kyokane T, Sano T, Suzuki H, Yamaguchi T, et al. Carbon monoxide-mediated alterations in paracellular permeability and vesicular transport in acetaminophen-treated perfused rat liver. HEPATOLOGY 1999;30:160-168.
6. Kyokane T, Norimizu S, Taniai H, Yamaguchi T, Takeoka S, Tsuchida E, et al. Carbon monoxide from heme catabolism protects against hepatobiliary dysfunction in endotoxin-treated rat liver. Gastroenterology 2001;120:1227-1240.
7. Zhao Y, Brandish PE, Ballou DP, Marletta MA. A molecular basis for nitric oxide sensing by soluble guanylate cyclase. Proc Natl Acad Sci U S A 1999;96:14753-14758.
8. Otterbein LE, Bach FH, Alam J, Soares M, Tao Lu H, Wysk M, et al. Carbon monoxide has anti-inflammatory effects involving the mitogen-activated protein kinase pathway. Nat Med 2000;6:422-428.
9. Abraham NG, Quan S, Mieyal PA, Yang L, Burke-Wolin T, Mingone CJ, et al. Modulation of cGMP by human HO-1 retrovirus gene transfer in pulmonary microvessel endothelial cells. Am J Physiol Lung Cell Mol Physiol 2002;283:L1117-L1124.
10. Hill M, Pereira V, Chauveau C, Zagani R, Remy S, Tesson L, et al. Heme oxygenase-1 inhibits rat and human breast cancer cell proliferation: mutual cross inhibition with indoleamine 2,3-dioxygenase. FASEB J 2005;19:1957-1968.
11. Thomas SR, Mohr D, Stocker R. Nitric oxide inhibits indoleamine 2,3-dioxygenase activity in interferon-gamma primed mononuclear phagocytes. J Biol Chem 1994;269:14457-14464.
12. Shinoda Y, Suematsu M, Wakabayashi Y, Suzuki T, Goda N, Saito S, et al. Carbon monoxide as a regulator of bile canalicular contractility in cultured rat hepatocytes. HEPATOLOGY 1998;28:286-295.
13. Wakabayashi Y, Takamiya R, Mizuki A, Kyokane T, Goda N, Yamaguchi T, et al. Carbon monoxide overproduced by heme oxygenase-1 causes a reduction of vascular resistance in perfused rat liver. Am J Physiol 1999;277:G1088-G1096.
14. Fujii K, Sakuragawa T, Kashiba M, Sugiura Y, Kondo M, Maruyama K, et al. Hydrogen sulfide as an endogenous modulator of biliary bicarbonate excretion in the rat liver. Antioxid Redox Signal 2005;7:788-794.
15. Vreman HJ, Wong RJ, Kadotani T, Stevenson DK. Determination of carbon monoxide (CO) in rodent tissue: effect of heme administration and environmental CO exposure. Anal Biochem 2005;341:280-289.

16. Motterlini R, Clark JE, Foresti R, Sarathchandra P, Mann BE, Green CJ. Carbon monoxide-releasing molecules: characterization of biochemical and vascular activities. Circ Res 2002;90:e17-e24.
17. Bossard R, Stieger B, O'Neill B, Fricker G, Meier PJ. Ethinylestradiol treatment induces multiple canalicular membrane transport alterations in rat liver. J Clin Invest 1993;91:2714-2720.
18. Soga T, Baran R, Suematsu M, Ueno Y, Ikeda S, Sakurakawa T, et al. Differential metabolomics reveals ophthalmic acid as an oxidative stress biomarker indicating hepatic glutathione consumption. J Biol Chem 2006;281:16768-16776.
19. Kinoshita A, Tsukada K, Soga T, Hishiki T, Ueno Y, Nakayama Y, et al. Roles of hemoglobin allostery in hypoxia-induced metabolic alterations in erythrocytes: simulation and its verification by metabolome analysis. J Biol Chem 2007;282:10731-10741.
20. Goda N, Suzuki K, Naito M, Takeoka S, Tsuchida E, Ishimura Y, et al. Distribution of heme oxygenase isoforms in rat liver: topographic basis for carbon monoxide-mediated microvascular relaxation. J Clin Invest 1998; 101:604-612.
21. Yonetani T, Tsuneshige A, Zhou Y, Chen X. Electron paramagnetic resonance and oxygen binding studies of alpha-nitrosyl hemoglobin: a novel oxygen carrier having NO-assisted allosteric functions. J Biol Chem 1998; 273:20323-20333.
22. Suganuma K, Tsukada K, Kashiba M, Tsuneshige A, Furukawa T, Kubota T, et al. Erythrocytes with T-state-stabilized hemoglobin as a therapeutic tool for postischemic liver dysfunction. Antioxid Redox Signal 2006;8: 1847-1855.
23. Meier M, Janosik M, Kery V, Kraus JP, Burkhard P. Structure of human cystathionine beta-synthase: a unique pyridoxal 5'-phosphate-dependent heme protein. EMBO J 2001;20:3910-3916.
24. Taoka S, Banerjee R. Characterization of NO binding to human cystathionine beta-synthase: possible implications of the effects of CO and NO binding to the human enzyme. J Inorg Biochem 2001;87:245-251.
25. Prudova A, Bauman Z, Braun A, Vitvitsky V, Lu SC, Banerjee R. S-adenosylmethionine stabilizes cystathionine beta-synthase and modulates redox capacity. Proc Natl Acad Sci USA 2006;103:6489-6494.
26. Zhao W, Zhang J, Lu Y, Wang R. The vasorelaxant effect of H_2S as a novel endogenous gaseous K_{ATP} channel opener. EMBO J 2001;20:6008-6016.
27. Werstuck GH, Lentz SR, Dayal S, Hossain GS, Sood SK, Shi YY, et al. Homocysteine-induced endoplasmic reticulum stress causes dysregulation of the cholesterol and triglyceride biosynthetic pathways. J Clin Invest 2001;107:1263-1273.
28. Maher JM, Dieter MZ, Aleksunes LM, Slitt AL, Guo G, Tanaka Y, et al. Oxidative and electrophilic stress induces multidrug resistance-associated protein transporters via the nuclear factor-E2-related factor-2 transcriptional pathway. HEPATOLOGY 2007;46:1597-1610.
29. Sasaki H, Sato H, Kuriyama-Matsumura K, Sato K, Maebara K, Wang H, et al. Electrophile response element-mediated induction of the cystine/glutamate exchange transporter gene expression. J Biol Chem 2002;277: 44765-44771.
30. Fiorucci S, Antonelli E, Mencarelli A, Orlandi S, Renga B, Rizzo G, et al. The third gas: H_2S regulates perfusion pressure in both the isolated and perfused normal rat liver and in cirrhosis. HEPATOLOGY 2005;42:539-548.
31. Suematsu M, Ishimura Y. The heme oxygenase-carbon monoxide system: a regulator of hepatobiliary function. HEPATOLOGY 2000;31:3-6.
32. Kato Y, Shimazu M, Kondo M, Uchida K, Kumamoto Y, Wakabayashi G, et al. Bilirubin rinse: a simple protectant against the rat liver graft injury mimicking heme oxygenase-1 preconditioning. HEPATOLOGY 2003;38:364-373.
33. Sano T, Shiomi M, Wakabayashi Y, Shinoda Y, Goda N, Yamaguchi T, et al. Endogenous carbon monoxide suppression stimulates bile acid-dependent biliary transport in perfused rat liver. Am J Physiol 1997;272:G1268-G1275.
34. Norimizu S, Kudo A, Kajimura M, Ishikawa K, Taniai H, Yamaguchi T, et al. Carbon monoxide stimulates mrp2-dependent excretion of bilirubin-IXα into bile in the perfused rat liver. Antioxid Redox Signal 2003;5:449-456.
35. Nathanson MH, Burgstahler AD, Mennone A, Dranoff JA, Rios-Velez L. Stimulation of bile duct epithelial secretion by glybenclamide in normal and cholestatic rat liver. J Clin Invest 1998;101:2665-2676.
36. Spirli C, Fiorotto R, Song L, Santos-Sacchi J, Okolicsanyi L, Masier S, et al. Glibenclamide stimulates fluid secretion in rodent cholangiocytes through a cystic fibrosis transmembrane conductance regulator-independent mechanism. Gastroenterology 2005;129:220-233.
37. Sellers ZM, Mann E, Smith A, Ko KH, Giannella R, Cohen MB, et al. Heat-stable enterotoxin of Escherichia coli (STa) can stimulate duodenal HCO_3^- secretion via a novel GC-C- and CFTR-independent pathway. FASEB J 2008;22:1306-1316.
38. Boon EM, Huang SH, Marletta MA. A molecular basis for NO selectivity in soluble guanylate cyclase. Nat Chem Biol 2005;1:53-59.
39. Kajimura M, Shimoyama M, Tsuyama S, Suzuki T, Kozaki S, Takenaka S, et al. Visualization of gaseous monoxide reception by soluble guanylate cyclase in the rat retina. FASEB J 2003;17:506-508.
40. Imai T, Morita T, Shindo T, Nagai R, Yazaki Y, Kurihara H, et al. Vascular smooth muscle cell-directed overexpression of heme oxygenase-1 elevates blood pressure through attenuation of nitric oxide-induced vasodilation in mice. Circ Res 2001;89:55-62.
41. Ishikawa M, Kajimura M, Adachi T, Maruyama K, Makino N, Goda N, et al. Carbon monoxide from heme oxygenase-2 is a tonic regulator against NO-dependent vasodilatation in the adult rat cerebral microcirculation. Circ Res 2005;97:e104-e114.

Microvascular Reviews and Communications

Vol.2 No.1

Three-dimensional imaging of growing thrombus *in vivo*

Takayuki Morikawa[1)] , Mayumi Kajimura[1),*], Mio Ichikawa[1)] , and Makoto Suematsu[1)]

1) Department of Biochemistry and Integrative Medical Biology, Keio University School of Medicine

Abstract

Although several methods have been developed to investigate thrombus or hemostatic plug formation in microvessels *in vivo*, our knowledge on platelet behavior during such a process is still limited. We, therefore, developed new instrumentation which enables us to induce interactions of individual platelets and to detect their behavior with endothelium in and around the growing thrombus. To evoke a platelet reaction, focal hemorrhage was induced with a nitrogen-dye laser focused through the microscope optics using mesenteric microcirculation of the rat. Platelet deposition at the site of injury was then observed during thrombus formation in real-time. The system was able to provide images with high spatial resolution at video-frame rate that could be used to reconstruct three-dimensional model of a thrombus. (Abstract movie) [MVRC **2**(1): 8-12,2008]

Key Words: thrombus formation, three-dimensional reconstruction, confocal, real-time, intravital microscopy

Received 2007/7/8, Accepted 2007/8/7

To whom correspondence should be addressed: Mayumi Kajimura, Department of Biochemistry and Integrative Medical Biology, Keio University School of Medicine
35 Shinano-machi, Shinjuku-ku, Tokyo160-8582, Japan
TEL: +81-3-3353-1211 (extension 63915) FAX: +81-3-3358-8138
E-mail: myk30@sc.itc.keio.ac.jp

Introduction

Process of thrombus or normal hemostatic plug formation upon vascular injury is initiated by the activation of circulating platelets. Biological and rheological properties of platelets have been extensively studied in the experimental systems *in vitro* such as in a parallel-plate flow chamber. Because platelet responses are affected by many factors in the normal environment, such as endothelium, other circulating cells, and blood flow *per se*, it is inevitable to examine such interactions *in vivo*. In this regard, several methods have been developed to evoke platelet activation and to observe thromboembolic process *in vivo*[1-3] . Among these, the most recent technology was developed by Falti *et al.*[3] with which vascular injury is induced by laser ablation technology and high-speed, near simultaneous acquisition of images of multiple fluorescent probes and the three-dimensional reconstruction of thrombus were made possible. Here we describe a new intravital imaging system that is essentially a modified technique of Falti *et al.*[3]. Because the system utilizes an analog 3CCD camera without using binning function, it was possible to acquire the image in real-time, i.e. 3 x 640 x 480 pixels format, 30 frames s^{-1} which enabled us to evaluate a single platelet behavior *in situ*.

Materials and Methods

Preparation of rats for intravital microscopy

Experiments were approved by the local ethical committee on the use of laboratory animals. Male Wistar rats (250-280 g; Clea Japan, Tokyo) were anesthetized with an intramuscular injection of sodium pentobarbital at 50 mg kg^{-1}, and the femoral vein was cannulated with a polyethylene catheter. Platelets circulating *in vivo* were labeled with an intravenous injection of carboxyfluorescein diacetate succinimidyl ester (CFDA-SE, Morikawa et al. Molecular Probes, Inc., Eugene, OR, USA) as described previously[4,5]. This compound is membrane-permeable and after it has entered cells it is hydrolyzed by esterase which predominantly occurs in platelets and leukocytes. After the dye infusion, the abdomen was opened and the ileocecal portion of the mesentery was arranged on the surface of the glass-coverslip for intravital observation. The mesentery was superfused continuously with the Krebs-Henseleit buffer saturated with 95% N_2/5% CO_2 at 2.0 ml min^{-1} at 37°C.

Thrombus generation by laser ablation of microvascular walls

Either an arteriole or a venule was chosen and endothelial injury was induced by a pulsed nitrogen-dye laser at 440 nm applied through the microscope objective using the MicroPoint laser system . Arterioles with a diameter of 15-30 μm or venules with that of 20-35 μm were targets for the injury.

Intravital imaging of thrombus formation

The imaging system constructed in this study is a modified method of Falati *et al.*[3]. The system was developed around an Olympus BX51W1 up-right microscope with a trinocular head (Olympus, Inc., Tokyo, Japan). Applications of the intravital microscopy in these experiments require either a 40 x (LUMPlanFI/IR, NA 0.8) or a 60 x (LUMFL, NA 1.1) water immersion lens. For confocal microscopy, we used a Yokogawa CSU21 confocal scanner (Yokogawa, Inc., Saitama, Japan) based on Nipkow disk technology. This confocal scanner uses the same pinholes for entrance and exit light beams but is also equipped with a second rotating disk that contains approximately 20,000 pinholes, each with a microlens. The disks rotate together at 1,800 rpm so that the light beams raster-scan the specimen. This technology allows the system to capture up to 360 flashed-frames s^{-1}. An argon-krypton two-line laser (Melles Griot, Carlsbad, CA, USA) provides the fluorescent light for confocal microscopy with excitation at 488 nm and 568 nm. The objective lens was mounted on a piezoelectric driver (Physik Instrumente-PZ73E, PI-Polytec CO., Ltd, Tokyo, Japan) which was controlled by a function generator (SG-4105, Iwatsu, Tokyo, Japan). A schematic representation of the instrumentation is shown in Figure 1.

To generate a laser-induced thrombus, the system was fitted with a nitrogen ablation laser (MicroPoint, Photonic Instruments, St. Charles, IL, USA) which was introduced via the epi-illumination port and was focused on the specimen through the microscope objectives. The output of the laser was at 337 nm but was subsequently tuned through a dye cell. We used coumarin as dye, which emits at 440nm. The laser delivers 4-nsec energy pulses, at a frequency between 3 and 10 Hz, over a surface approximately 1-μm in diameter; the energy of the pulses can be controlled by the operator. In order to conduct consistent ablation, the objective lens was kept at a stationary position until we became certain about a

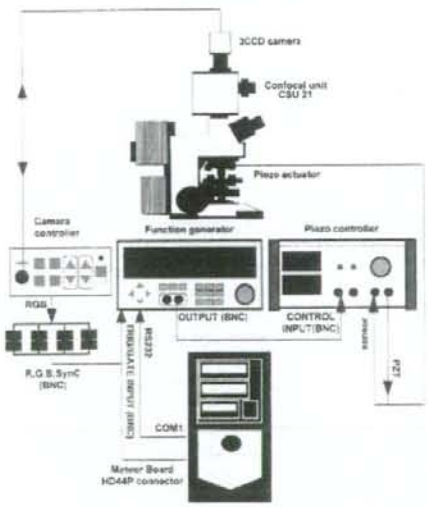

Fig.1 Schematic representation of the experimental setup. See text in Materials and Methods for details.

successful ablation. The ablation was considered successful if erythrocytes left from the vessel, indicating that all components of the vessel layers were damaged. We then started to operate a piezoelectric driver which allows very fine movement in the vertical direction of the sample.

Video acquisition and three-dimensional reconstruction of developing thrombus

The central part of the trinocular stand was connected to an analog color CCD camera (JK-TU52H, Toshiba, Tokyo) that allowed us to record color images with acceptable spatial and temporal resolutions (640 x 480 pixels format, 30 frames s^{-1}). Analog signals were digitized via a frame grabber (Meteor-II, Matrox Electronic Systems Ltd, Tokyo). The computer had a 3 GHz processor, 1 GB of RAM, and three SCSI hard drives including one 160GB-RAID-0. This computer system was capable to acquire real-time color images for the duration of approximately 90 min. Using a piezo-electric driver on an objective lens, optical slices are obtained. Imaging software (StreamPix ver. 3.7.0, Norpix Inc., Montreal, Quebec, Canada) was used to control the hardware components during image acquisition. Finally acquired images were stacked to generate a three-dimensional reconstruction of a developing thrombus by three kinds of imaging software; StreamPix, IP Lab (ver. 3.6.4, Scanalytics, Inc., Fairfax, VA, USA) and Vox Blast (ver. 3.0, VayTek, Inc., Fairfield, Iowa, USA).

Results

Tissue depth of the formed images

Figure 2 shows a representative image of a three-dimensional reconstruction. Here we first positioned the microscope lens at the center of the venule, namely at the point where the largest diameter was seen. The position of the lens was then moved upwards by 22.5 μm and images composed of 640 x 480 pixels with 1.5-μm steps for the total depth of 45 μm were collected. The 45-μm height of the images was intentionally greater than the diameter of the venule in order to compensate for inexact positioning of the lens before the start of the experiment. As seen in Panel A of the x-z section which transverses to the microvessels on this mesentery, only the top half of the circumference of this venule, but not the bottom half of it was visualized. When the dissecting plane was moved 18.7-μm more deeply (Panel B), the shape of the platelet thrombus on this venular wall became apparent. However, when a further 18.3-μm deeper section was made (Panel C), the system failed to form a sharp image. The result suggests a limitation of this optic system as a whole on the tissue depth of image acquisition which was approximately a 30-μm depth from the tissue surface. Therefore microvessels and thrombi residing in the superficial layer lying no more than 30 μm from the surface were subjected to this study.

Thrombus formation upon laser ablation

Upon the injury by laser ablation, a thrombus started to form typically over a 20 second to 1 min period. Thereafter either did it remain rather constant in size

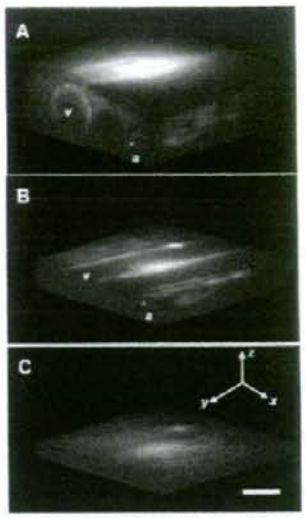

Fig.2 Three-dimensional images of CFSE-associated fluorescence at 10 min after the initial ablation of the venule. At each x-y confocal plane, a 2D image was obtained and these images were stacked in sequential order with an imaging-software to yield a 3D images of the rat mesentery. The image seen in panel A was reconstituted from twenty-eight different x-y planes covered 45-μm depth of the tissue, and each images are 1.5- μm apart. The x-y dissecting plane was moved 18.7-μm (panel B), and further 18.3-μm more deeply (panel C). Scale bar=30 μm. a, arteriole; v, venule.

with producing small emboli or it embolized as a whole cluster and started to form another thrombus. A small population of platelets tethering at the growing thrombus appeared to change their shape from normal discoid to flattened morphology. Figure 3 (Movie 1) shows such a process between 20 seconds and 40 seconds after the start of laser ablation. Spatial distribution of platelets in and around the thrombus was evaluated by three-dimensional reconstruction.

Figure 4 (Movie 2) and Figure 5 (Movie 3) are the representative three-dimensional images where the scan was made on the longitudinal or radial axis of the venule, respectively. As seen, the optical resolution of the system was sufficient to visualize the interaction between the growing thrombus and circulating platelets on this

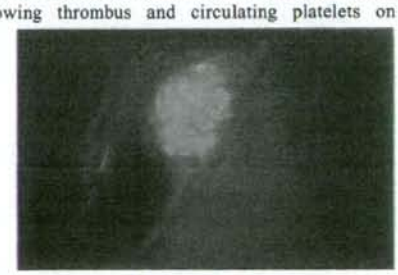

Fig.3(Movie 1) Developing thrombus upon laser ablation on a venule. Two dimensional images were acquired between 20 seconds and 40 seconds after the start of laser ablation. Towards the end of this movie, the whole thrombus embolized.

Fig.4(Movie 2) Three-dimensional reconstruction of a thrombus induced by laser ablation on a venule. Spatial distribution of platelets in the thrombus was evaluated by this scanning. Scans were made on the x-z plane (vertical) traversing the longitudinal axis of the microvessels. Note that single platelets in the thrombus were visualized.

Fig.5(Movie 3) Three-dimensional reconstruction of a thrombus induced by laser ablation on a venule. Spatial distribution of platelets in the thrombus was evaluated by this scanning. Scans were made radially on the x-y plane (horizontal) from the top surface to the approximately the centerline of this venule.

venule.

Figure 6 shows temporal changes in thrombus shape. At 0 second, the initial image showed minimal fluorescence. At 20 seconds, platelets started to accumulate on the point of injury on the vessel wall. At 26 seconds, the platelet thrombus expanded further.

Discussion

In the present study, we established an intravital imaging system with which the platelet interaction can be visualized in real-time during thrombus formation on the mesenteric microcirculation. The optical-and the time-resolution of the system were sufficient to visualize the interaction between the growing thrombus and circulating platelets under the current condition. Utilizing an analog camera system offers the advantage that thrombus formation is visualized on-line with high resolution. This approach therefore enabled us to obtain three-dimensional geometry of the growing thrombus and to study the kinetics of thrombus growth *in vivo*.

To examine the process of thrombus formation, assessment must be ideally performed vertically as well as horizontally through the whole volume of a thrombus. The current system enables to rapidly acquire the information for a thrombus residing in the superficial layer lying no more than 30 μm from the mesenteric surface. It could be speculated that due to the light scattering properties of the imaged tissue, confocal images often suffer from significant intensity attenuation in deeper parts of the specimen[6,7]. The reason could be that both the laser as well as the emitted light are

Fig.6 Three-dimensional reconstruction of a growing thrombus showing temporal changes in shape and volume. At each x-y confocal plane, a 2D image was obtained and these images were stacked in sequential order with an imaging-software to yield a 3D image. Representative images of different x-y planes covered 28-μm depth of the tissue, and each images were 1-μm apart. Bar=10 μm.

absorbed and scattered more in deeper parts of the specimen than in parts near the objective lens. This could have caused a greater rejection of the light from the sample to form the image through an array of microlens of Nipkow spinning disk.

Despite the non-ideality of this system discussed above, the system is able to acquire high-spatial resolution images with video-frame rate that can provide us important information to analyze platelet behavior *in vivo*. As seen in Figure 3 (Movie 1), the system is capable of acquiring very sharp images of individual platelets at the site of growing thrombus. Although circulating free flow platelets were rapidly moving, time resolution appears to be appropriate to detect the behavior of tethering and/or adherent platelets of which are the majority in and around a thrombus without severe blur along the longitudinal axis of the vessel (Fig. 4 and 5 (Movie 2 and 3)).

With the laser-induced injury, we observed that as soon as the endothelium was damaged by the laser, platelets rapidly started to accumulate to form a hemostatic plug which was confined at the injured site (Fig. 6). Our methodology allowed us to examine process and content of growing thrombus at the sites of injured vasculature. At present, our system is equipped to capture two different fluorophores that can be excited by 488 nm and 568 nm without crossover of fluorescence. To gain the insight for the kinetics of growing thrombus, its laser source and filter systems should be developed further to visualize the components of growing thrombus other than platelets, e.g. fibrin and tissue factors, which was accomplished by the system of Falati *et al*[3]. In conclusion, the current instrumentation enables us to unravel the biological and rheological properties of single platelet behavior in and around a developing thrombus *in vivo*.

Acknowledgements

This work was supported by Health Labour Sciences Research Grant, Research on Advanced Medical Technology from the Ministry of Health Labour and Welfare (to M.K.), and Grant-in-Aid for Creative Scientific Research, Leading Project for Biosimulation, the 21st Century Center-of-Excellence Program from the Ministry of Education, Culture, Sports, Science and Technology in Japan (to M.S.). Our gratitude goes to Mr. Toshihiro Ochiai who immensely helped us to make this system work.

References

1) Arfors KE., Dhall DP., Engeset J., Hint H., Matheson NA., Tangen O.: Biolaser Endothelial Trauma as a Means of Quantifying Platelet Activity *in vivo*. *Nature*. **218**: 887-888, 1968.
2) oude Egbrink MG., Tangelder GJ., Slaaf DW., Reneman RS.: Thromboembolic reaction following wall puncture in arterioles and venules of the rabbit mesentery. *Thromb Haemost*. **59**: 23-28, 1988.
3) Falati S., Gross P., Merrill-Skoloff G., Furie BC., Furie B.: Real-time *in vivo* imaging of platelets, tissue factor and fibrin during arterial thrombus formation in the mouse. *Nat Med*. 8: 1175-1180, 2002.
4) Katayama T., Ikeda Y., Handa M., Tamatani T., Sakamoto S., Ito M., Ishimura Y., Suematsu M.: Immunoneutralization of glycoprotein Ibalpha attenuates endotoxin-induced interactions of platelets and leukocytes with rat venular endothelium *in vivo*. *Circ Res*. **86**: 1031-1037, 2000.
5) Suematsu M., DeLano FA., Poole D., Engler RL., Miyasaka M., Zweifach BW., Schmid-Schonbein GW.: Spatial and temporal correlation between leukocyte behavior and cell injury in postischemic rat skeletal muscle microcirculation. *Lab Invest*. **70**: 684-695, 1994.
6) Shen CL., Scott GL., Merchant F., Murphy RM.. Light scattering analysis of fibril growth from the amino-terminal fragment beta(1-28) of beta-amyloid peptide. *Biophys J*. **65**: 2383-2395, 1993.
7) Hell S., Reiner G., Cremer C, Stelzer EHK.: Aberrations in confocal fluorescence microscopy induced by mismatches in refractive index. *J Microscopy*. **169**: 391-405,1993.

Circ J 2009; **73:** 540–548

Important Regulatory Role of Activated Platelet-Derived Procoagulant Activity in the Propagation of Thrombi Formed Under Arterial Blood Flow Conditions

Noriko Tamura, MS; Isao Kitajima, MD**; Yota Kawamura, MD; Eri Toda, MD; Yu Eguchi, MD; Hideyuki Ishida, MD*; Shinya Goto, MD

Background: The functional links between the activation of platelets and the coagulation system have not been clarified.

Methods and Results: Immobilized collagen fibrils were perfused with human blood containing fluorescinated platelets in the presence of various concentrations of thrombin inhibitor. Coagulant activity around platelet thrombi was detected using a FITC-conjugated antibody against the fibrin monomer complex (F-405). Intra-cytosolic calcium ion concentrations ($[Ca^{2+}]_i$) in individual platelets and the volume of thrombi were detected with an ultrafast confocal laser microscope equipped with a piezo-motor control unit. The volume of platelet thrombi formed after 8 min of blood perfusion in the presence of 10, 25, 50, and 100 μmol/L argatroban was 7.69±0.46 μm^3, 6.61±1.96 μm^3, 3.63±1.54 μm^3, and 1.67±0.75 μm^3, respectively. There was a positive correlation between the volume of platelet thrombi and the amount of fibrin monomer complex produced around them. The $[Ca^{2+}]_i$ of the platelets forming the thrombi oscillated between a minimum of 92.0±57.4 nmol/L, 120.1±68.1 nmol/L, and a maximum of 217.6±131.5 nmol/L, 367.6±189.1 nmol/L, respectively, in the presence of 100 and 10 μmol/L argatroban.

Conclusions: The results suggest a crucial role of coagulant activity in both the generation of fibrin and the growth of platelet thrombi. (*Circ J* 2009; **73:** 540–548)

Key Words: Blood flow; Calcium; Fibrin monomer complex; Platelet; Thrombin

Thrombi causing the "so-called atherothrombotic diseases"[1] contain at least 3 components: platelets, fibrin, and inflammatory cells[2,3] The functions and activation mechanisms of the platelets[4,5] the coagulation cascade[6,7] and the inflammatory cells[8] have been investigated extensively. Now, attention is being focused on the functional links among these components during the formation of thrombi large enough to cause symptomatic atherothrombosis[9,10–13]

Indeed, platelets adhere and accumulate at sites of endothelial damage and are known to play a central role in the local regulation of coagulation and inflammation (eg, platelets have a procoagulant membrane component on their surface upon activation[14,15] express adhesive molecules[16] to capture inflammatory cells in the thrombi, release inflammatory cytokines such as the CD40 ligand[17–19] and procoagulant microparticles[20,21]). Local activation of coagulation and inflammation that occurs around the activated platelets themselves may influence the functions of the platelets through stimulation of various receptors, such as protease-activated receptors (mostly PAR1, but also PAR4[22]),[23] ADP receptors[14] integrins[24] etc); however, these mechanisms are still not fully understood[1,11,12]

In the present study, we investigated the functional interrelationships between platelets and the coagulation system under arterial blood flow conditions, although the later is believed to be activated in vivo mostly at sites of blood stagnation.

(Received May 16, 2008; revised manuscript received October 7, 2008; accepted October 19, 2008; released online January 29, 2009)

*Department of Medicine, *Department of Basic Science, Tokai University School of Medicine, Isehara and **Department of Clinical Laboratory and Molecular Pathology, University of Toyama, Toyama, Japan*

Mailing address: Shinya Goto, MD, Department of Medicine, Tokai University School of Medicine, 143 Shimokasuya, Isehara 259-1143, Japan. E-mail: sgoto3@mac.com

Methods

Preparation of Blood Samples, Artificial Blood Flow Conditions, and Measurement of the $[Ca^{2+}]_i$ of Platelets Incorporated in Thrombi

Venous blood samples were collected from 10 adult volunteers after obtaining their written informed consent. The investigation conformed with the principles of the Declaration of Helsinki and the study protocol was approved by the Internal Review Board of Tokai University. All of the study subjects (8 men, 2 women; age 28–44 years) were instructed to abstain from drugs known to interfere with platelet function during the month preceding the study. The blood specimens were immediately transferred into plastic tubes containing 1/10 volume of the specific thrombin inhibitor argatroban (Mitsubishi Kagaku, Tokyo, Japan) at final concentrations ranging from 10 to 100 μmol/L, to test for antithrombin effects on the formation of fibrin around the

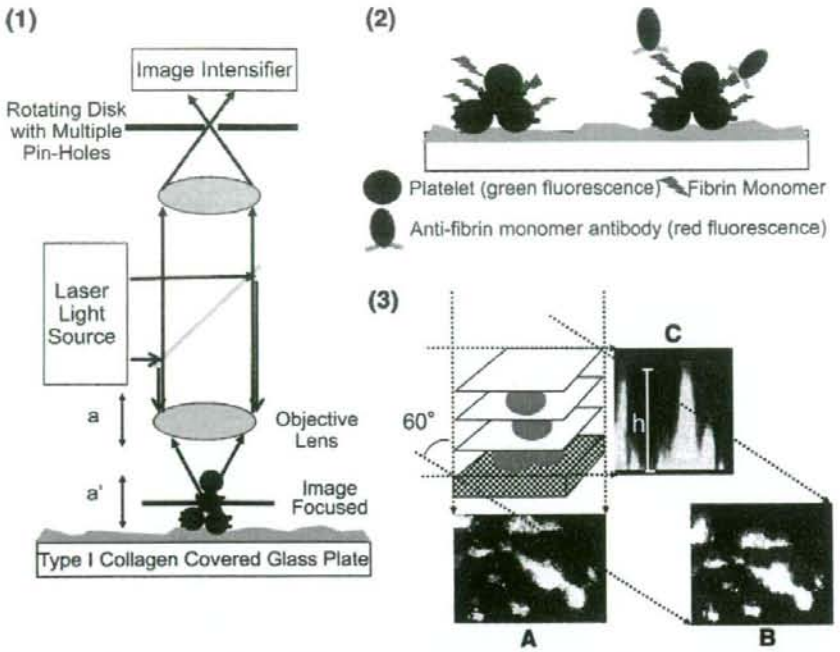

Figure 1. Multicolor and 3-dimensional (D) imaging of the thrombi formed under arterial blood flow conditions. Type I collagen fibrils were perfused with blood containing fluoresceinated platelets for 8 min at a wall shear rate of 1,500/s in a rectangular flow chamber. Thrombi formed on the collagen fibrils were visualized using both an epi-fluorescent multicolor video-microscope and the newly developed ultra-fast confocal laser microscope equipped with a piezo-motor control unit, as depicted schematically on the left-hand side. The activation of platelet-derived procoagulant activity was detected as the appearance of the fibrin monomer complex around the platelet thrombi visualized (in red), while platelets were visualized in green. The objective lens was moved up and down at a constant speed of 0.4 μm/s under the control of the piezo-motor control unit (a) to obtain scanning images of the platelet thrombi (a'). The sum of the scanning confocal images from the bottom to the top was projected on planes at 10-degree intervals relative to the x-axis to obtain the 3-D projection images shown on the right-hand side, including the projections at 0 degrees (top view, **A**), 60 degrees (**B**) and 90 degrees (front view, **C**). The maximum height (h) of the platelet thrombi was calculated from the frontal projection image, as shown in **C**.

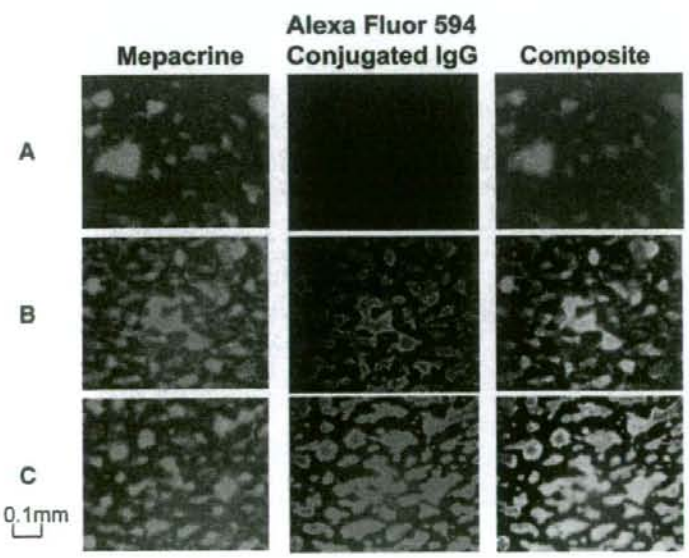

Figure 2. Specific detection of the fibrin monomer complex around the platelet thrombi. Platelet thrombi formed as a result of perfusion of the collagen fibrils with whole blood for 8 min (Left). Next, they were incubated with HEPES-NaCl solution (pH 7.4) containing either 1 of the monoclonal antibodies, negative control antibody against thyroglobulin (T_γ), human fibrin monomer complex (F-405), or positive control antibody against the platelet surface protein GPIbα (GUR20-5) at a concentration of 5 μg/ml for 15 min. The specificity of the red fluorescence staining in the presence of anti-human fibrin monomer complex antibody (**B**) was confirmed by comparison with the staining results obtained with negative (**A**) and positive (**C**) control antibody. Superimposition of the green and red fluorescence staining images revealed the prominent presence of the fibrin monomer complex on the surface of the platelet thrombi.

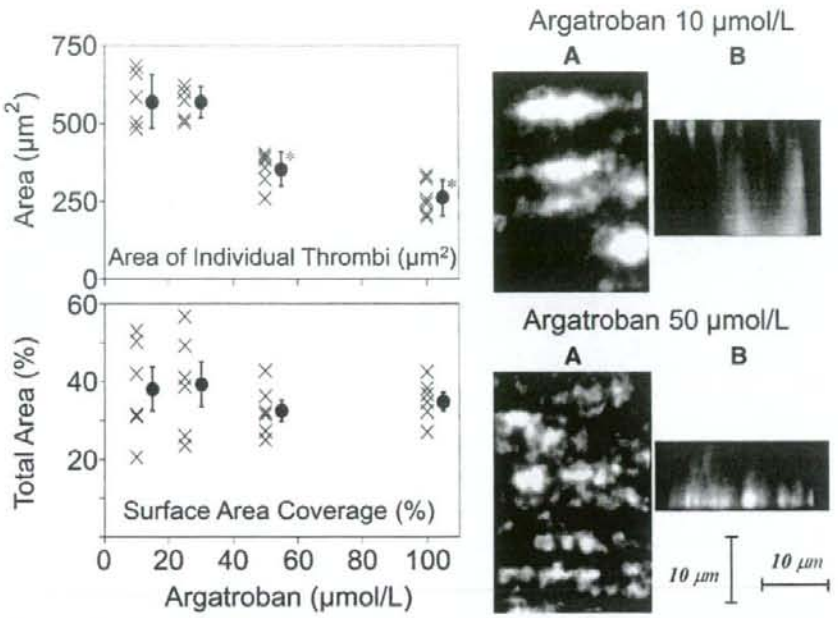

Figure 3. Relationship between inhibition of the function of thrombin and the 2- and 3-dimensional (D) growth of the platelet thrombi formed on the collagen fibrils by blood perfusion at a wall shear rate of 1,500/s. Immobilized collagen fibrils in the rectangular flow chamber were perfused with blood samples containing the specific thrombin inhibitor argatroban (10–100 μmol/L) at varying final concentrations for 8 min at a wall shear rate of 1,500/s. Projection images at (**A**) 0 degrees along the x-axis corresponding to the projection from the top of the thrombi and (**B**) 90 degrees along the x-axis corresponding to the projection from the side of the thrombi. Quantitative results obtained from these 3-D images are summarized in Table 1. Quantitative surface area coverage by individual platelet thrombi, (**Lower left**) total area covered by the platelets. The results demonstrate the mean and standard error of 6 different experiments. *Significantly smaller value than that obtained by 8 min of perfusion of blood containing the lowest concentration of antithrombin tested in the study (10 μmol/L).

Table 1. Surface Area Coverage, Height and Volume of Individual Thrombi Formed on the Collagen Fibrils After 8 min of Perfusion of Blood Containing Various Concentrations of Antithrombin

Argatroban (μmol/L)	10	25	50	100
Area (μm^2)	576.7±–81.3	555.0±181.4	359.1±111.1*	256.7±47.3*
Height (μm)	17.6±2.8	14.9±1.6	13.7±3.0*	10.4±0.6*
Volume (mm^3)	7.69±0.46	6.61±1.96	3.63±1.54*	1.67±0.75*

*Value is significantly smaller than that obtained after 8 min of perfusion of blood containing the lowest concentration of argatroban used in the study (10 μmol/L). The same value is significantly smaller than that obtained in the presence of 25 or 50 μmol/L of argatroban.

platelet thrombi, on calcium signaling, and on the growth of the platelet thrombi[25–27] Clinically relevant anticoagulants, including unfractionated heparin and low-molecular-weight heparin, were also tested, but the results could not be included because the blood coagulated during experiments.

For the experiments conducted to examine the growth of the thrombi and imaging of the platelet-derived procoagulant activity, platelets in whole blood samples were rendered fluorescent by the addition of mepacrine (Sigma Chemical Co, St Louis, MO, USA)[25,27,28] For the experiments conducted to measure the intra-cytosolic calcium ion concentrations ($[Ca^{2+}]_i$), the platelets were loaded with the calcium-sensitive dye, fluo-3AM, in accordance with a previously described procedure[29] with slight modification[26] Fluo-3 loaded platelets were re-suspended in homologous, initially separated platelet-poor plasma containing the antithrombin agent argatroban at a concentration of 10 or 100 μmol/L. The hematocrit of the final cell suspension was adjusted to 40%.

A rectangular flow chamber with its glass bottom coated with immobilized type I collagen fibrils was assembled as described previously![4,25,28] The experimental blood samples were aspirated into the chamber with a syringe pump (Harvard Apparatus, Holliston, MA, USA) for 8 min at a constant flow rate to obtain a wall shear rate of 1,500/s unless otherwise specified (limited number of experiments were conducted at shear rate 0 and 100/s).

Imaging of the Platelet Thrombi and Measurement of Platelet-Derived Procoagulant Activity

The platelet thrombi were initially visualized using an inverted-stage epi-fluorescence video-microscopy system connected to a 480-nm excitation light source (DM IRB, 1RB-FLUO, Leica, Germany)![4,25] To quantify the 2-dimensional (D) growth of the platelet thrombi, both the surface

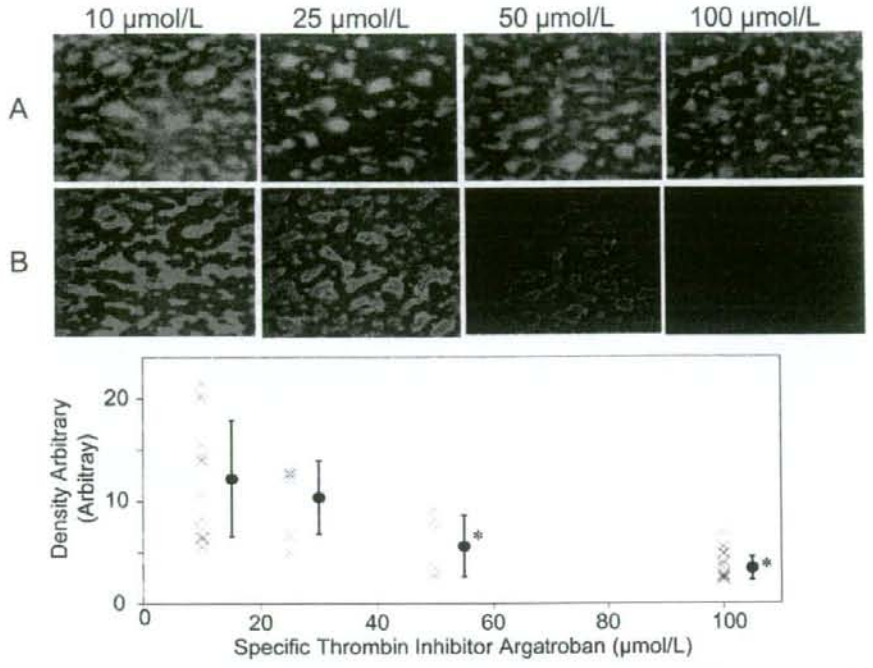

Figure 4. Relationship between functional inhibition of thrombin and the generation of the fibrin monomer complex around the platelet thrombi. The experiments were conducted in a similar manner as described in Figure 3. Dual-color fluorescence imaging was performed after washing with secondary antibody 3 times with 5 ml of HEPES-NaCl solution (pH 7.4). Fluoresceinated platelets (green), and fibrin monomers (red) were visualized using a barrier filter centered at the wavelengths of 527 nm (**A**) and 600 nm (**B**), respectively. Quantitative densitometry was performed to detect the total amount of fibrin monomers formed around the platelet thrombi, and the results are summarized in the lower panel.

area coverage of individual platelet thrombi (μm^2) and the total surface area coverage of the platelets (%) were calculated.[25] The 3-D projection images of the platelet thrombi were also obtained with a fast confocal laser microscope equipped with a piezo-motor control unit, as described previously[26,30,31] (**Figure 1**). The 3-D projection images of the thrombi were obtained using the ImageJ 1.29v program (National Institutes of Health, Bethesda, MD, USA), as shown in **Figure 1**.[26,30,31] The maximum height of the thrombi was calculated from a 90-degree (front) projection image, and the volume of each thrombus was derived by integration of the cumulative cross-sectional area occupied by the platelets in confocal sections obtained at 0.2-μm intervals.

For imaging of the activation of the coagulation cascade on the surface of the platelet thrombi (platelet-derived procoagulant activity), HEPES-NaCl solution (pH 7.4) containing mouse-derived monoclonal antibody against the human fibrin monomer complex F-405[32] at a final concentration of 5 μg/ml was incubated with the platelet thrombi formed after 8 min of blood perfusion (**Figure 1**). The presence of the anti-fibrin monomer complex antibody on the platelet thrombi was detected using Alexafluor594-conjugated goat-derived anti-mouse polyclonal IgG (Molecular Probes, Inc, OR, USA) at a final concentration of 10 μg/ml. Both FITC-conjugated Annexin V (kindly provided by Dr Nomura, Kansai University, Osaka, Japan) and Alexafluor594-conjugated monoclonal antibody against tissue factor ATN-8 (kindly provided by Chugai, Co Ltd, Gotenba, Japan) were used in some experiments to detect the distribution of negatively charged phospholipids and/or tissue factor on and/or around the platelet thrombi.[15,33] Dual-color fluorescence imaging, to detect platelets as green and the fibrin monomer complex as red, was performed after the washing procedure with a barrier filter centered at wavelengths of 527 nm and 600 nm, respectively (**Figure 2**). The specificity of detection of the fibrin monomer complex by this method was confirmed by comparison with the same concentration of iso-type matched negative and positive control IgG (GUR20-5: antibody against platelet GPIbα, kindly provided by Dr Handa, Keio University, Tokyo, Japan) as shown in **Figure 2**. Quantitative densitometry was performed to measure the total amount of fibrin monomer complex formed around the platelet thrombi using the same method as that described previously to estimate the amount of platelet accumulation.[27]

Real-Time Imaging to Measure $[Ca^{2+}]_i$ in Platelets Forming Thrombi Under Blood Flow Conditions

The $[Ca^{2+}]_i$ of the platelets forming thrombi was measured using the same confocal microscopy system described previously,[29,26] but without the use of the piezo-motor control unit. Variations in the fluorescence intensity of the fluo-3AM-loaded platelets were converted into $[Ca^{2+}]_i$ using the equation:

$$[Ca^{2+}]_i = Kd(F - Fmin)/(Fmax - F),$$

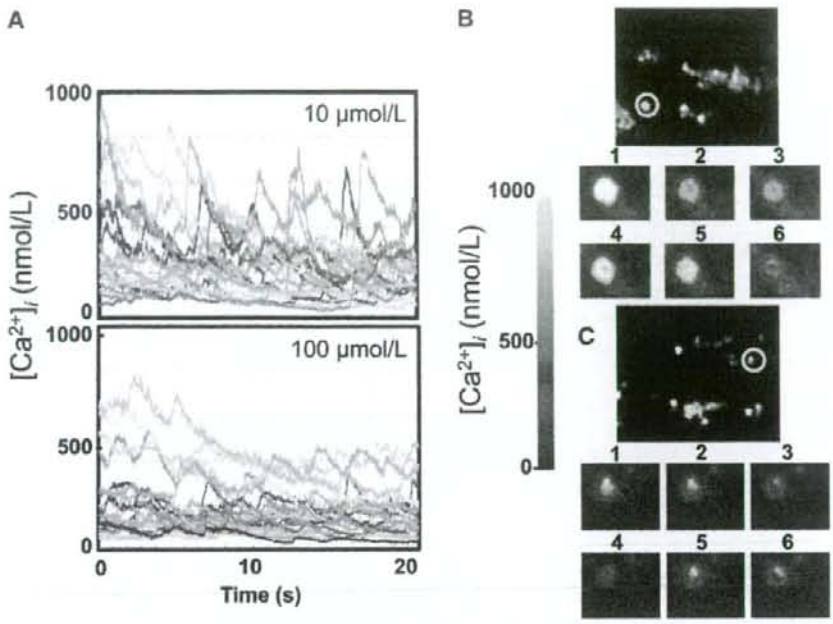

Figure 5. Changes in the $[Ca^{2+}]_i$ of the platelets forming the thrombi on the collagen fibrils under blood flow conditions. These experiments were conducted as described in Figure 3, except that the blood was replaced with a cell suspension containing fluo-3AM-loaded platelets, washed erythrocytes and homologous platelet-poor plasma with the specific thrombin inhibitor argatroban at 2 different concentrations, 10 and 100 μmol/L. (**Left**: **A**) $[Ca^{2+}]_i$ of 10 randomly selected platelets recorded over a 10-s period beginning 2 min after the start of the blood perfusion, (**Right**) fluorescence images reflecting the $[Ca^{2+}]_i$ in individual platelets starting to adhere to the collagen surface in the presence of 10 μmol/L (**B**) and 100 μmol/L (**C**) of specific thrombin inhibitor argatroban. The results shown are representative of 4 different experiments.

where Kd is the dissociation constant of fluo-3AM in the interaction with Ca^{2+} (corresponding to 495 nmol/L at 25°C)[34] F is the measured fluorescence intensity of a single platelet, Fmax is the fluorescence intensity of a single platelet treated with the Ca^{2+} ionophore A23187 (10 μmol/L; Sigma) in the presence of 2 mmol/L calcium chloride, and Fmin is the fluorescence intensity of an unstimulated single platelet. To examine whether the changes in the $[Ca^{2+}]_i$ were related to trans-membrane entry or changes in the intracellular distribution, the effects of lanthanum chloride, a putative calcium-channel blocker, were tested[26,35]

Statistical Analysis

All numerical data are expressed as mean ± SD, unless otherwise specified. The effect of various concentrations of argatroban on the growth of the platelet thrombi was tested by 1-way analysis of variance (ANOVA). Differences between 2 groups of data were evaluated by Newman-Keuls test; $P<0.05$ was considered to denote statistical significance.

Results

Inter-Relationship Between Inhibition of the Coagulation Cascade and Growth of Platelet Thrombi

As shown in **Figure 3**, the size of the individual thrombi that formed on the collagen fibrils was smaller after perfusion of blood containing higher concentrations of thrombin inhibitor. Quantitative analysis revealed that the area covered by individual platelet thrombi in the presence of thrombin inhibitor at concentrations of 50 and 100 μmol/L was significantly smaller than that formed in the presence of 10 μmol/L ($P<0.05$), as shown in **Figure 3** and **Table 1**. The total surface area covered by the platelets was not significantly influenced by the concentration of thrombin inhibitor, indicating that a larger number of smaller thrombi formed in the presence of higher concentrations of thrombin inhibitor.

The 3-D projection imaging of the platelet thrombi using our newly developed confocal imaging technique revealed that the height and volume of individual thrombi formed after 8 min of perfusion of blood containing lower concentrations of thrombin inhibitor were larger than those formed after perfusion of blood containing higher concentrations of the same inhibitor (**Figure 3**, **Table 1**).

Activation of the Coagulant Cascade Around Activated Platelets and the Role in Maintaining the Activated State of Platelets Incorporated Into Thrombi Under Arterial Blood Flow Conditions

As shown in the upper panels of **Figure 4**, there was a larger amount of fibrin monomer complex, detected as red fluorescence, around the platelet thrombi formed in the presence of lower concentrations of thrombin inhibitor. A similar distribution of FITC-conjugated Annexin V could be detected under the same conditions, whereas neither tissue factor nor tissue-factor-bearing microparticles, a homogeneous distribution of which could be detected by our imaging system, were detected around the platelet thrombi (data not shown). Quantitative densitometric analysis, shown

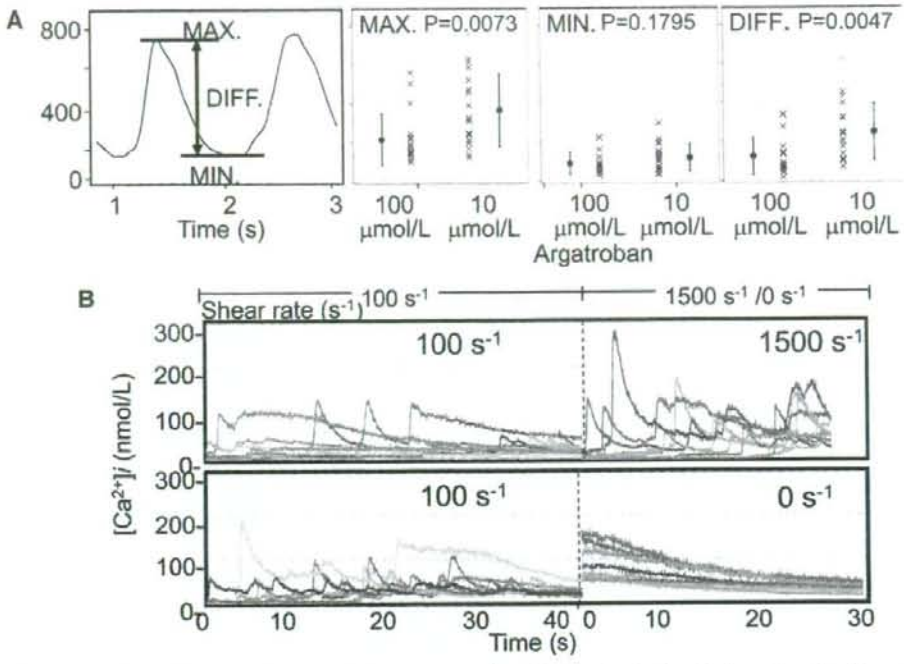

Figure 6. Quantitative results of $[Ca^{2+}]_i$ and changes in the $[Ca^{2+}]_i$ of the platelets forming the thrombi on the collagen fibrils under various shear rates. (**A**) These experiments were conducted as described in Figure 6. The minimum (MIN.), maximum (MAX.) and difference (DIFF.) between the minimum and maximum $[Ca^{2+}]_i$ defined in the upper right panel were calculated for 20 randomly selected platelets in 4 different experiments. The mean values and the SD are shown. (**B**) These experiments were conducted as described in Figure 6, except that the shear rate was changed as shown in the upper panel. Each line represents the $[Ca^{2+}]_i$ in individual platelets under shear rates shown above. Results shown are the 4 different experiments in the presence of 100 μmol/L of specific thrombin inhibitor argatroban.

in the lower panel of **Figure 4**, demonstrates the dose-dependent inhibitory effects of thrombin inhibitor on the generation of the fibrin monomer complex around the platelet thrombi formed under arterial blood flow conditions.

The $[Ca^{2+}]_i$ of the platelets adhering to the collagen fibrils is shown in **Figure 5A**. A cyclic increase in the $[Ca^{2+}]_i$ occurred in the majority of individual platelets adhering to the immobilized collagen fibrils, although the strength and cycle length of the oscillations were not homogeneous. The addition of the putative calcium-channel blocker, lanthanum chloride, at a final concentration of 1 mmol/L to the blood samples completely blocked these cyclic increases in the $[Ca^{2+}]_i$[26] (data not shown). There was, however, a tendency for the maximum increase in the $[Ca^{2+}]_i$ to be greater in the presence of lower concentrations of thrombin inhibitor. Indeed, quantitative analysis of 20 randomly selected platelets in 4 different experiments revealed that both the maximum value and the differences between the maximum and minimum values of $[Ca^{2+}]_i$ were significantly higher in the presence of 10 μmol/L argatroban than the corresponding values in the presence of 100 μmol/L of the same inhibitor (**Figure 6A**). We also demonstrated that the cyclic increase in the $[Ca^{2+}]_i$ is shear rate dependent and disappears at a shear rate of 0 (**Figure 6B**).

Discussion

In the present study, we demonstrated activation of the coagulation cascade around platelet thrombi formed under arterial blood flow conditions, as evidenced by the appearance of fibrin monomer complexes around the platelet thrombi. We have also demonstrated that the cyclic increase in $[Ca^{2+}]_i$ in each platelet incorporated into the thrombi, which is assumed to represent the sum of the activation signals of the platelet and has been shown to be influenced by shear rate and the presence of specific thrombin inhibitor, positively correlates with the 3-D growth, especially in the z-section, of the platelet thrombi. Our experimental results suggest an important regulatory role of thrombin generated on the surface of activated platelets as a result of the procoagulant activity in both the formation of fibrin around the platelets and the maintenance of the activated state of platelets incorporated into thrombi so that the platelet thrombi remain stable and, at least in our experimental conditions, the calcium-sensitive phospholipid scramblase[36,37] is activated to continue further expression of procoagulant phospholipid on the platelet thrombi (**Figure 7**)[38,39]

Our experimental results with human blood samples were in complete agreement with in vivo animal experiments published previously[33] Our findings fundamentally serve to confirm those animal experimental results, except that we used human blood in an in vitro setup without blood vessels. Obviously, our model does not pose any problems related to species differences, which is important in understanding the regulatory role of the activation of the coagulant cascade in the 3-D growth of platelet thrombi, because it is well